Minimum Specific Energy and Transcritical Flow in Unsteady Open-Channel Flow

Oscar Castro-Orgaz[1] and Hubert Chanson[2]

Abstract: The study and computation of free surface flows is of paramount importance in hydraulic and irrigation engineering. These flows are computed using mass and momentum conservation equations, their solutions exhibiting special features depending on whether the local Froude number (F) is below or above unity, thereby resulting in wave propagation in the upstream and downstream directions or only in the downstream direction, respectively. This dynamic condition is referred to in the literature as *critical flow* and is fundamental to the study of unsteady flows. Critical flow is also defined as the state at which the specific energy and momentum reach a minimum, based on steady-state computations, and it is further asserted that the backwater equation gives infinite free surface slopes at control sections. So far, these statements were not demonstrated within the context of an unsteady-flow analysis, to be conducted in this paper for the first time. It is demonstrated that the effects of unsteadiness break down critical flow as a generalized open-channel flow concept, and correct interpretations of critical flow, free surface slopes at controls, minimum specific energy, and momentum are given within the context of general unsteady-flow motion in this paper. **DOI: 10.1061/(ASCE)IR.1943-4774.0000926.** *© 2015 American Society of Civil Engineers.*

Author keywords: Critical flow condition; Open channel; Transcritical flow; Water discharge measurement; Unsteady flow; Weir.

Introduction

Shallow open-channel flows occur in a wide range of engineering problems including irrigation canals, dam spillways, or drainage channels. These flows are mathematically computed using vertically integrated conservation equations of mass and momentum assuming that the pressure distribution is hydrostatic (Yen 1973, 1975; Liggett 1993; Montes 1998). Free surface flows are classified as subcritical or supercritical depending on whether the local Froude number (F) is above or below the threshold value $\mathsf{F} = 1$, respectively. The limiting value $\mathsf{F} = 1$ is a dynamic criterion, defining critical flow as the flow condition for which the mean flow velocity exactly equals the celerity of an elementary gravity wave (Liggett 1993, 1994). Critical flow is defined by the following simultaneous properties in the literature (Chow 1959; Henderson 1966; Montes 1998; Hager 1999; Jain 2001; Sturm 2001; Chanson 2004; Chaudhry 2008): (1) specific energy is minimum (Bakhmeteff 1932; Jaeger 1949); (2) mean flow velocity equals the celerity of a small gravity wave (Stoker 1957; Liggett 1993); (3) specific force reaches a minimum (Jaeger 1949; Chow 1959); (4) water surface slope is infinite in the steady backwater equation (Bélanger 1828; Henderson 1966); and (5) discharge per unit width is maximum, as used in the design of minimum energy loss (MEL) culverts (Apelt 1983; Chanson 2004). These properties may be also extended to nonhydrostatic pressure fields (Chanson 2006). The five conditions stated are linked in the literature as simultaneous conditions defining critical flow as a unique dynamic state. However, a number of critiques may be raised:

1. Critical depth in a rectangular channel is $h_c = (q^2/g)^{1/3}$, with q as the unit discharge. This depth originates by setting $dE/dh = 0$ in the specific energy definition $E[= h + q^2/(2gh^2)]$, or $dS/dh = 0$ in the specific force or specific momentum expression $S[= h^2/2 + q^2/(gh)]$. The minimum values, $E_{\min}$ and $S_{\min}$ corresponding to h_c are obtained assuming that the flow is steady (Jaeger 1949). However, critical flow, defined as $\mathsf{F} = 1$, is obtained by setting the slope of the unsteady backward characteristic curve $dx/dt = U - (gh)^{1/2} = 0$ (Liggett 1993), from which $U = (gh)^{1/2}$, where $\mathsf{F} = U/(gh)^{1/2}$ is the Froude number, $U = q/h$ is the mean flow velocity, x is the longitudinal coordinate, t is time, and h is the water depth. This results from an unsteady-flow analysis, in contradiction to the steady-flow analysis, while computing the extremes of E and S.
2. Unsteady computation of transcritical flows using the Saint-Venant equations lacks from infinite free surface slopes away from shocks (Toro 2002). This is not in agreement with the backwater equation for steady flow that always predicts $dh/dx \to \infty$ at critical flow. This is a paradox because the backwater equation is a simplification for steady state of the unsteady Saint-Venant equations (Chanson 2004), from which both should be identical.

These observations indicate that the effect of unsteadiness on critical flow was so far not investigated. This paper was designed to fill in this gap because critical flow is one of the most important concepts upon which the theory of open-channel flow relies. The first objective of this paper is to verify the computation of the steady transcritical water surface profiles over variable topography, with weir flow as a representative test case, using the gradually varied flow equation assisted by the singular point method to remove the indetermination at the critical point, because of the lack of general acceptance of this method in the hydraulics community. Unsteady-flow computations using a finite-volume model are conducted to compute the asymptotic steady-flow profile starting from another steady state. The asymptotic unsteady-flow computations

[1]Professor of Hydraulic Engineering, Univ. of Cordoba, Campus Rabanales, Leonardo Da Vinci Building, E-14071 Cordoba, Spain (corresponding author). E-mail: oscarcastro@ias.csic.es; ag2caoro@uco.es

[2]Professor in Hydraulic Engineering, School of Civil Engineering, Univ. of Queensland, Brisbane, QLD 4072, Australia. E-mail: h.chanson@uq.edu.au

Note. This manuscript was submitted on December 21, 2014; approved on April 28, 2015; published online on July 2, 2015. Discussion period open until December 2, 2015; separate discussions must be submitted for individual papers. This paper is part of the ***Journal of Irrigation and Drainage Engineering***, © ASCE, ISSN 0733-9437/04015030(12)/$25.00.

are then used to track whether a singular point is formed in the computational domain as steady state is approached. Unsteady-flow results are further used to compute numerically the water surface slope at the channel control to its comparison with the corresponding steady-state solution using L'Hopital's rule. This analysis will serve to decide if the backwater equation is associated with singularities that can be handled using L'Hopital's rule or, in contrast, with an infinity free surface slope, as normally assumed in the literature.

The second objective of this paper is to investigate whether critical flow is a unique dynamic state in transient flows. Following Liggett (1993), the definition of critical flow should specify the point at which the equations of motion (both steady and unsteady) are singular. Liggett (1993) further indicated that the critical depth could be defined by minimizing the specific energy, but such a definition would not expose the singularities in the equations of motion and, therefore, would have little use. However, no proof or discussion of these differences was given so far. As pointed out previously, the definition of critical flow using the continuity and momentum equations in unsteady flow [$dx/dt = 0$, with $q = q(x,t)$ and $h = h(x,t)$] is not coherent with the steady definition of critical flow as the state for which the specific energy becomes a minimum [$dE/dh = 0$, with q = const and $h = h(x)$]. This is in close agreement with the statements of Liggett (1993). This point is especially important because all hydraulic books so far available and used for teaching and research in open-channel hydraulics implicitly assume that both conditions are equivalent, without any analytical or numerical proof. Thus, general unsteady-flow computations of transcritical flow over a weir are conducted in this paper to compute the evolution of $E(x,t)$, $\mathsf{F}(x,t)$, and $S(x,t)$ in the x-t computational domain. The aim of these computations is to investigate whether the point $\mathsf{F} = 1$ ($dx/dt = 0$) generally agrees with the points where E and S reach a minimum value. Further, critical flow (defined as the maximum discharge for a given specific energy) permits the definition of head-discharge relationships used for discharge measurement purposes (Bos 1976; Chanson 2004). Computation of the relationship between discharge and specific energy at a weir crest during unsteady flow will reveal whether the maximum discharge condition applies for water discharge measurement. This paper, therefore, will reveal if critical flow can be defined as a unique flow state in transient flows or if the effect of unsteadiness is to break down critical flow as a generalized open-channel flow concept.

Steady Flow

Governing Equations

Steady state shallow water open-channel flows are computed using the gradually varied flow equation (Chow 1959; Henderson 1966; Jain 2001; Sturm 2001; Chanson 2004)

$$\frac{dh}{dx} = \frac{S_o - S_f}{1 - \mathsf{F}^2} \tag{1}$$

where S_o = channel slope; and S_f = friction slope. For the sake of simplicity, a rectangular cross section of constant width is considered in this paper. Eq. (1) is a first order differential equation that must be solved subjected to one boundary condition that is a known flow depth for a given discharge (Chaudhry 2008). The specific energy E in open-channel flow is defined as (Bakhmeteff 1912, 1932; Chow 1959; Henderson 1966)

$$E = h + \frac{U^2}{2g} = h + \frac{q^2}{2gh^2} \tag{2}$$

It is well known that the minimum specific energy $dE/dh = 0$ is reached at the critical depth $h_c = (q^2/g)^{1/3}$ (Henderson 1966), where the specific momentum $S = h^2/2 + q^2/(gh)$ also reaches a minimum value (Jaeger 1949). Inserting this depth into the definition of F yields $U = (gh)^{1/2}$ and $dh/dx \to \infty$ in Eq. (1). The consequence is that it is routinely stated in the literature that the gradually varied flow equation breaks down at the critical flow condition. In an attempt to justify that from a physical standpoint, one argument is that near the critical depth the pressure is nonhydrostatic; and therefore, Eq. (1) is invalid. However, the mathematical validity of Eq. (1) at a critical point is different from the physical correctness of the gradually varied flow theory if pressure is not hydrostatic, as detailed in the next section. The Belanger-Böss theorem (Jaeger 1949; Montes 1998) states the equivalence of $dE/dh = 0$ for q = const and $dq/dh = 0$ for E = const. Thus, the discharge becomes a maximum for the given specific energy head under critical flow in steady flows.

Singular Point Method

An important case of transcritical open-channel flow is the passage from subcritical ($\mathsf{F} < 1$) to supercritical ($\mathsf{F} > 1$) flow over variable topography, typically over a weir (Fig. 1). Let $z_b(x)$ be the bed profile and assume that the flow is frictionless (i.e., $S_f = 0$) so that Eq. (1) reduces to

$$\frac{dh}{dx} = \frac{-\frac{\partial z_b}{\partial x}}{1 - \mathsf{F}^2} \tag{3}$$

An infinite free surface slope is not observed experimentally in transcritical flow over a weir (Blau 1963; Wilkinson 1974; Hager 1985; Chanson and Montes 1998; Chanson 2006). If $\mathsf{F} = 1$, then Eq. (3) must equal the indeterminate identity $dh/dx = 0/0$. This automatically fixes the critical point at the weir crest $\partial z_b/\partial x = 0$ (Hager 1985, 1999). However, the value of dh/dx remains unknown, although the slope is definitely not infinite. This singularity is removed by applying L'Hospital's rule to Eq. (3), resulting in (Massé 1938; Escoffier 1958)

$$\left(\frac{dh}{dx}\right)_c = \pm\left(-\frac{h_c}{3}\frac{\partial^2 z_b}{\partial x^2}\right)^{1/2} \tag{4}$$

This technique, to remove flow depth gradients of the kind $0/0$ on the shallow-water steady-state equations, is known as

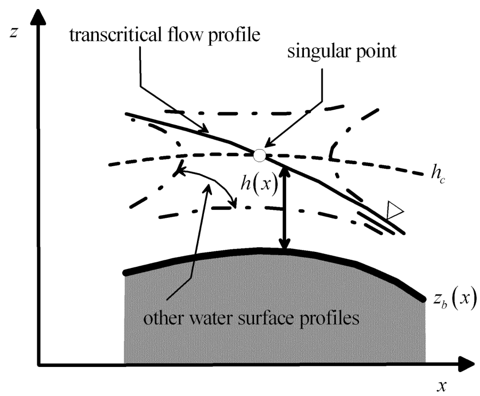

Fig. 1. Transcritical flow profile over variable topography: formation of steady singular point

the singular point method. It originates from the work of Poincaré (1881) on ODE equations and was applied to open channel transition flow problems by Massé (1938), Escoffier (1958), Iwasa (1958), Wilson (1969), and Chen and Dracos (1996). However, this method is rarely accepted by open-channel flow workers because the argument still prevails that Eq. (1) is invalid for $h = h_c$ given the existence of a nonhydrostatic pressure distribution. As discussed previously, the gradually varied flow model is mathematically valid at the critical depth, but it is physically inaccurate if the flow curvature is high (Montes 1998). The singular point method is rarely explained in open-channel flow books, with Chow (1959) and Montes (1998) as exceptions. However, mathematical books often describe it for general application in engineering (i.e., von Kármán and Biot 1940). Because of the lack of general acceptance of the singular point method for the steady gradually varied flow equation, its validity will be assessed using general unsteady-flow computations to produce an asymptotic steady state. This will permit to track whether a singular point is asymptotically formed in the computational domain as a steady state is approached.

Unsteady Flow

Governing Equations

One-dimensional unsteady shallow water flows are described by the Saint-Venant equations, written in conservative vector form (Vreugdenhil 1994; Chaudhry 2008)

$$\frac{\partial \mathbf{U}}{\partial t} + \frac{\partial \mathbf{F}}{\partial x} = \mathbf{S} \tag{5}$$

where $\mathbf{U}$ = vector of conserved variables; $\mathbf{F}$ = flux vector; and $\mathbf{S}$ = source term vector, given by

$$\mathbf{U} = \begin{pmatrix} h \\ hU \end{pmatrix}; \qquad \mathbf{F} = \begin{pmatrix} hU \\ hU^2 + \frac{1}{2}gh^2 \end{pmatrix};$$

$$\mathbf{S} = \begin{bmatrix} 0 \\ gh\left(-\frac{\partial z_b}{\partial x} - S_f\right) \end{bmatrix} \tag{6}$$

Again, Eq. (5) is based on the assumption of hydrostatic pressure. It can be solved to compute the transcritical flow profile over variable topography subjected to suitable initial and boundary conditions. A steady-flow profile can be simulated using unsteady-flow computations until an equilibrium state is obtained as given by the corresponding boundary and initial conditions. Modern shock-capturing methods like the finite-volume method apply to produce transcritical flow profiles over variable topography without any additional special care or technique as the flow passes across the point $h = h_c$. This unsteady-flow computation of a free surface profile can be therefore compared with the steady-state computation based on Eq. (3), assisted by Eq. (4) to remove the singularity at the critical point. The unsteady-flow computations can also be used to compute the asymptotic steady free surface slope at the critical point and, then, to compare the numerical estimates with the analytical steady-state solution given by Eq. (4). Further, during the transient flow, the functions $E = E(x,t)$, $S = S(x,t)$, and $\mathsf{F} = \mathsf{F}(x,t)$ can be tracked to detail their evolution as functions of both time and space. It will serve to highlight whether steady-state definitions of critical flow (i.e., $E = E_{\min}$ and $S = S_{\min}$) apply to unsteady-flow motion and agree with the unsteady critical flow condition $dx/dt = 0$ (or $\mathsf{F} = 1$). The numerical computations used in this paper are described in the "Numerical Method of Solution" section.

Numerical Method of Solution

Among the possible methods of solution for Eq. (5) the finite-volume method was selected. Shock capturing finite-volume solutions using the Godunov upwind method assisted by robust Riemann solvers (approximate or exact) are well established today as accurate solutions of shallow-water flows (Toro 2002; LeVeque 2002). The integral form of Eq. (5) over a control volume is (Toro 1997, 2002)

$$\int_{\Omega} \frac{\partial \mathbf{U}}{\partial t} d\Omega + \int_{A} \mathbf{n} \cdot \mathbf{F} dA = \int_{\Omega} \mathbf{S} d\Omega \tag{7}$$

where Ω = control volume; A = cell boundary area; and $\mathbf{n}$ = outward unit vector normal to A. Choosing a quadrilateral control volume in the x-t plane, the conservative Eq. (7) reads (Toro 2002)

$$\mathbf{U}_i^{n+1} = \mathbf{U}_i^n - \frac{\Delta t}{\Delta x}(\mathbf{F}_{i+1/2} - \mathbf{F}_{i-1/2}) + \Delta t \mathbf{S}_i \tag{8}$$

where n = time level; i = cell index in the x-direction; and $\mathbf{F}_{i+1/2}$ = numerical flux crossing the interface between cells i and $i+1$ [Fig. 2(a)]. Source terms $\mathbf{S}_i$ and the fluxes $\mathbf{F}_{i+1/2}$ are evaluated at a suitable time level depending on the specific method. In this paper, the MUSCL-Hancock method is used (Toro 1997, 2002), which is second-order accurate in both space and time. Specific aspects of the method are detailed subsequently.

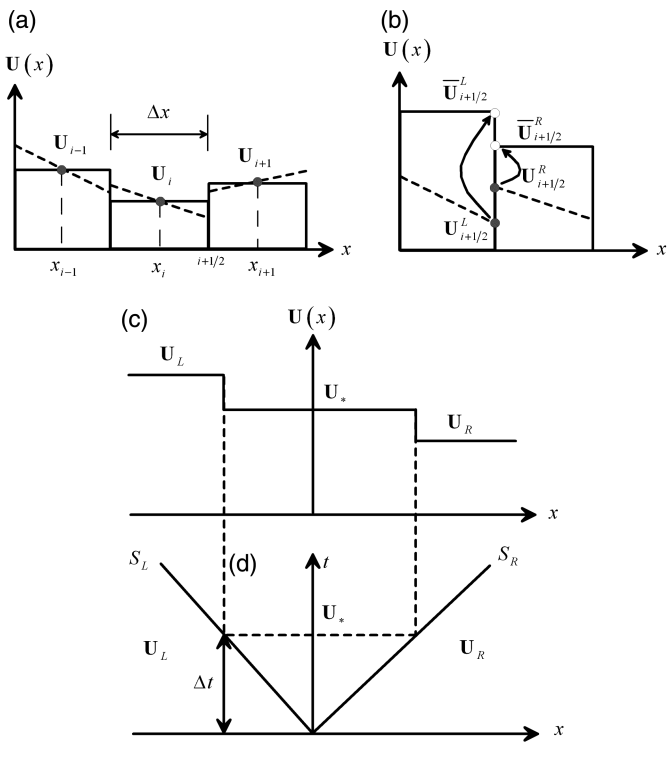

Fig. 2. Finite-volume solution using MUSCL-Hancock method: (a) linear reconstruction within each cell; (b) evolution of boundary extrapolated values; HLL Riemann solver for each interface in (c) ($\mathbf{U}$-x) plane; (d) (x-t) plane

Reconstruction of Solution

The solution process starts with the cell-averaged values of conserved variables at time level n, $\mathbf{U}_i^n$. To obtain second-order accuracy in space, a piecewise linear reconstruction is made within each cell (Toro 2002) [Fig. 2(a)]. Linear slopes resulting from the reconstructed solution must be limited to avoid spurious oscillations near discontinuities. Letters L and R denote the reconstructed variables at the left and right sides of a cell interface, so that the resulting values of $\mathbf{U}$ at each of its sides are with $\Phi_{i-1/2}^+$ and $\Phi_{i-3/2}^-$ as diagonal limiter matrices (Toro 2002)

$$\mathbf{U}_{i+1/2}^L = \mathbf{U}_i^n + \frac{1}{2}\Phi_{i-1/2}^+(\mathbf{U}_i^n - \mathbf{U}_{i-1}^n);$$
$$\mathbf{U}_{i+1/2}^R = \mathbf{U}_{i+1}^n - \frac{1}{2}\Phi_{i+3/2}^-(\mathbf{U}_{i+2}^n - \mathbf{U}_{i+1}^n) \tag{9}$$

A Minmod limiter is used in all computations presented in this paper. Further, Eq. (9) implies that the water depths at each time level n are reconstructed. This technique is denoted as the depth-gradient method (Aureli et al. 2008). Another option is to use the auxiliary vector $\mathbf{Q} = (h + z_b, Uh)$ instead of $\mathbf{U} = (h, Uh)$. The reason is that reconstruction using water depths may lead to nonphysical flows over variable topography under static conditions, an issue that is fully resolved if the reconstruction is based on the water surface elevation $z_s = h + z_b$ (Zhou et al. 2001) by using a suitable bottom source term discretization. However, as pointed out by Aureli et al. (2008), the surface gradient method may lead to oscillations and nonphysical depths (even negative) for shallow supercritical flows. In contrast, the depth-gradient method is more stable and robust for bore front tracking. During this paper, both methods were applied to transcritical flow over weirs; the surface gradient method leads in some cases to unstable results in the tailwater supercritical portion of the weir face, in agreement with the results of Aureli et al. (2008). In contrast, the results using the depth-gradient method were found accurate enough, and, thus, results based on that technique are presented in this paper.

Numerical Flux

The computation of the numerical flux $\mathbf{F}_{i+1/2}$ at each interface requires knowledge of boundary-extrapolated values of variables at the left and right sides of the interface $\mathbf{U}_{i+1/2}^L$ and $\mathbf{U}_{i+1/2}^R$. In the MUSCL-Hancock method, an additional step is added rendering a nonconservative evolution of boundary extrapolated values $\mathbf{U}_{i+1/2}^L$ and $\mathbf{U}_{i+1/2}^R$ at interface $i + 1/2$ over half the time step, to regain second-order accuracy in time as [Fig. 2(b)]

$$\bar{\mathbf{U}}_{i+1/2}^L = \mathbf{U}_{i+1/2}^L - \frac{\Delta t}{2\Delta x}[\mathbf{F}(\mathbf{U}_{i+1/2}^L) - \mathbf{F}(\mathbf{U}_{i-1/2}^R)] + \frac{\Delta t}{2}\mathbf{S}_i;$$
$$\bar{\mathbf{U}}_{i+1/2}^R = \mathbf{U}_{i+1/2}^R - \frac{\Delta t}{2\Delta x}[\mathbf{F}(\mathbf{U}_{i+3/2}^L) - \mathbf{F}(\mathbf{U}_{i+1/2}^R)] + \frac{\Delta t}{2}\mathbf{S}_{i+1} \tag{10}$$

With these evolved boundary extrapolated variables $\bar{\mathbf{U}}_{i+1/2}^L$ and $\bar{\mathbf{U}}_{i+1/2}^R$ defining states L and R, the numerical flux is computed using the HLL approximate Riemann solver [Fig. 2(c)] as (Toro 2002)

$$\mathbf{F}_{i+1/2} = \begin{cases} \mathbf{F}_L & \text{if } S_L \geq 0 \\ \dfrac{S_R\mathbf{F}_L - S_L\mathbf{F}_R + S_R S_L(\mathbf{U}_R - \mathbf{U}_L)}{S_R - S_L} & \text{if } S_L \leq 0 \leq S_R \\ \mathbf{F}_R & \text{if } S_R \leq 0 \end{cases} \tag{11}$$

where $\mathbf{F}_L$ and $\mathbf{F}_R$ =fluxes computed at states L and R. Robust wave speeds estimates S_L and S_R [Fig. 2(d)] are given by (Toro 2002)

$$S_L = U_L - a_L q_L; \qquad S_R = U_R + a_R q_R \tag{12}$$

where $a = (gh)^{1/2}$; and $q_K (K = L, R)$ is

$$q_K = \begin{cases} \left\{\frac{1}{2}\left[\frac{h_*(h_* + h_K)}{h_K^2}\right]\right\}^{1/2} & h_* > h_K \\ 1 & h_* \leq h_K \end{cases} \tag{13}$$

The flow depth at the start region of the Riemann problem at each interface h_* is (Toro 2002)

$$h_* = \frac{1}{g}\left[\frac{1}{2}(a_L + a_R) + \frac{1}{4}(U_L - U_R)\right]^2 \tag{14}$$

Time Stepping

For stability in time of the explicit scheme, the Courant-Friedrichs-Lewy (CFL) number must be less than unity (Toro 1997, 2002). For selection of the time step, CFL was fixed to 0.9 in this paper and Δt was determined at time level n using the equation

$$\Delta t = \mathrm{CFL}\left[\frac{\Delta x}{\max|U_i^n + (gh_i^n)^{1/2}|}\right] \tag{15}$$

where Δt and Δx = step sizes in the t and x axes, respectively.

Source Terms

The computation of shallow-water flow over variable topography must be conducted using a well-balanced scheme. It implies that once a discretization is applied to the source terms, the time evolution of the conserved variables must reach a stable steady state $\mathbf{U}_i^{n+1} = \mathbf{U}_i^n$ if afforded by the boundary conditions. That is, the asymptotic steady-state version of Eq. (8)

$$(\mathbf{F}_{i+1/2} - \mathbf{F}_{i-1/2}) + \Delta x\mathbf{S}_i = \mathbf{0} \tag{16}$$

may be regarded as an identity that is verified only if the discretization of $\mathbf{S}$ is correctly done. For the MUSCL-Hancock scheme using the surface gradient method, a well-balanced discretization of the bottom slope term is (Zhou et al. 2001)

$$h\frac{\partial z_b}{\partial x} \approx \left(\frac{h_i^L + h_i^R}{2}\right)\frac{(z_{bi+1/2} - z_{bi-1/2})}{\Delta x} \tag{17}$$

implying that the bed profile is linearly distributed within a cell, with a mean bed elevation for cell i given by

$$z_{bi} = \frac{z_{bi+1/2} + z_{bi-1/2}}{2} \tag{18}$$

For the depth-gradient method, the model would give nonphysical flows under static conditions however. Static tests resulted in discharges of less than 10^{-5} m^2/s for the weirs simulated, so that the model was considered accurate enough. In the numerical literature, passing a static test ($q = 0$) is considered an index of good predictions of steady-state solutions. However, it does not imply, in general, that the identity given by Eq. (16) is verified for any discharge $q \neq 0$. So, in turn, an unsteady numerical model must be checked and compared with steady-state solutions, as done in this paper.

Initial Conditions

The test cases considered in this paper are weir flows of parabolic and Gaussian shapes. Specific details of each weir tested are given in the “Results” section. An initial steady free surface profile over the weir, for which q = constant and $h = h(x)$ is known, must be prescribed to initiate unsteady computations. In this paper, Eq. (1) was used to produce an initial free surface profile for a low discharge over the weir, i.e., $q = 0.01\ \mathrm{m^2/s}$. The profile was numerically computed using the fourth-order Runge-Kutta method (Chaudhry 2008). Computations started at the crest section, where $h = h_c$. At this section, Eq. (4) was implemented in the Runge-Kutta solver, and the corresponding subcritical and supercritical branches of the water surface profile were computed in the upstream and downstream directions, respectively.

Boundary Conditions

For transcritical flow over a weir, one boundary condition must be prescribed at the subcritical section on the upstream weir side; whereas at the supercritical outlet section no boundary conditions need to be prescribed. The inlet boundary condition is given by an instantaneous rise in the discharge, which is kept constant during all the transient flow. Unknown values of conserved variables at boundary sections are then computed using ghost cells by extrapolation of values at adjacent interior cells (LeVeque 2002). The use of ghost cells is a common technique in finite-volume methods and gives results that are accurate (LeVeque 2002; Ying et al. 2004).

Alternative Solution

In this paper, the MUSCL-Hancock method was further compared with the one-sided upwind finite-volume method of Ying et al. (2004). In this model the Saint-Venant equations are recast with z_s as the free surface elevation in the form

$$\mathbf{U} = \begin{pmatrix} h \\ hU \end{pmatrix}; \quad \mathbf{F} = \begin{pmatrix} hU \\ hU^2 \end{pmatrix}; \quad \mathbf{S} = \begin{bmatrix} 0 \\ gh\left(-\dfrac{\partial z_s}{\partial x} - S_f\right) \end{bmatrix} \tag{19}$$

With this formulation, the model equations automatically pass the still water numerical test (Ying et al. 2004). The gradient $\partial z_s/\partial x$ is computed on the basis of the Courant number, as given by Ying et al. (2004), and the numerical flux is

$$\mathbf{F}_{i+1/2} = \begin{cases} q_{i+k}^n \\ \dfrac{(q_{i+k}^n)^2}{h_{i+k}^n} \end{cases} \tag{20}$$

where $k = 0$, if q_i and $q_{i+1} > 0$; $k = 1$, if q_i and $q_{i+1} < 0$; $k = 1/2$ for any other case; and where $i + 1/2$ refers to an average of the values at the i and $i + 1$ grid points.

Accuracy of Saint-Venant Equations for Variable Topography

For steady frictionless flow over a weir, Eq. (1) or Eq. (5) are equivalent to conservation of the total energy head H as

$$H = z_b + h + \frac{q^2}{2gh^2} \tag{21}$$

This equation gives smooth mathematical solutions for transcritical flow over a weir and is consistent with the formation of steady singular points asymptotically during an unsteady flow. However, these issues are related to the mathematical possibility of computing transcritical flows using gradually varied flow models, but not to the physical accuracy or correctness of the theory itself. One aspect widely criticized in the water discharge measurement literature is that for weir flows the pressure is nonhydrostatic, making Eq. (21) invalid (Blau 1963; Bos 1976; Hager 1985; Montes 1994; Chanson 2006; Castro-Orgaz 2013). In contrast, numerical literature widely uses the transcritical flow over a weir as a performance test of numerical schemes for solving the Saint-Venant equations. Thus, their validity for variable bed topography is examined in this paper. Matthew (1991), using Picard’s iteration technique, obtained with the subindex indicating ordinary differentiation with respect to x the second-order equation for potential free surface flow as

$$H = z_b + h + \frac{q^2}{2gh^2}\left(1 + \frac{2hh_{xx} - h_x^2}{3} + hz_{xx} + z_{bx}^2\right) \tag{22}$$

This is a second-order differential equation describing the flow depth profile $h = h(x)$. For its solution, an initial value of H is adopted, and the upstream boundary flow depth is computed as the subcritical root of Eq. (21). The free surface slope is set to zero at that section. Using these boundary conditions, Eq. (22) is integrated using the fourth-order Runge-Kutta method. The upstream head must be iterated until the supercritical root of Eq. (21) is reached at the tailwater section.

Results

Steady Water Surface Profiles

The steady water surface profile over a weir of bed shape $z_b = 0.2 - 0.01x^2$ (m) was computed for a target discharge of $q = 0.18\ \mathrm{m^2/s}$ using the MUSCL-Hancock method, and the results are shown in Fig. 3(a). This particular weir is widely used to test unsteady numerical models (i.e., Zhou et al. 2001; Ying et al. 2004). In this case, $\Delta x = 0.05$ m and CFL $= 0.9$ were used. The results

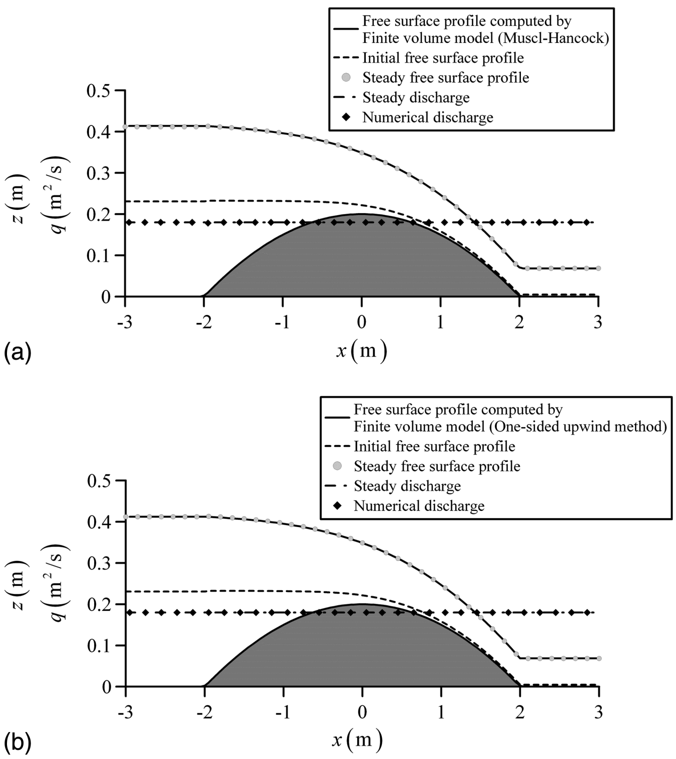

Fig. 3. Finite-volume solution of flow over parabolic weir by (a) MUSCL-Hancock scheme; (b) one-sided upwind scheme

presented in the figure correspond to a simulation time of $t = 50$ s. The steady water surface profile computed using Eqs. (3) and (4) is presented in the same figure, showing excellent agreement with the finite-volume computation. This suggests that the application of the singular point method correctly produces the transcritical flow profile over variable topography. As further observed, the discharge is conserved with good accuracy by the unsteady-flow model. The same computations were conducted in Fig. 3(b) using the one-sided upwind finite-volume method, with results almost identical (the two profiles deviate in the third decimal position) to those using the MUSCL-Hancock method, justifying the use of the depth-gradient method in this paper.

Water Surface Slope at Critical Point

The unsteady-flow model was used to compute numerically the water surface slope at the weir crest at any instant of time to second-order accuracy as

$$\left(\frac{dh}{dx}\right)_c \approx \frac{(h_{i+1} - h_{i-1})}{2\Delta x} \tag{23}$$

Computational simulations until reaching a steady state over the weir were conducted for varying discharges at the weir inlet. The unsteady numerical results at $t = 50$ s, obtained from Eq. (23) are plotted in Fig. 4 together with the analytical steady state Eq. (4). Both results almost perfectly match, thereby indicating that the unsteady flow over a weir produces a singular point asymptotically in the crest section as the steady state is approached. This demonstrates that the singular point method is a correct mathematical tool permitting to remove indeterminations in the computational domain as the flow passes from subcritical to supercritical. This technique permits to mimic with a steady-state computation what shock-capturing unsteady computations automatically do. Experimental data of Wilkinson (1974) for steady flow over cylindrical weirs are plotted in Fig. 4, indicating the accuracy of the Saint-Venant theory in predicting the free surface slope at the control section up to $-h_c z_{bxx} = 0.15$. Following Wilkinson (1974), the accuracy of water surface slope computations using the singular point method is restricted to the limit $-h_c z_{bxx} \approx 0.25$, given the curvilinear flow over the crest domain. The accuracy of the theory is further exploited subsequently by considering the existence of a nonhydrostatic pressure.

Accuracy of Saint-Venant Theory

Fig. 5 contains the experimental data of Sivakumaran et al. (1983) for a Gaussian hump of profile $z_b = 20\exp[-0.5(x/24)^2]$ (cm) for two test cases. The computed Saint-Venant solution using the finite-volume method is presented for both cases and compared in Fig. 5 with the nonhydrostatic steady-flow computations using Eq. (22). The clear departure between the two for the test case of Fig. 5(a) ($E_{\min}/R = 0.516$, $q = 0.111$ m^2/s) indicates that the effect of the vertical acceleration as the flow passes from subcritical to supercritical is significant, so that the Saint-Venant theory does not apply despite the flow being shallow. For the test case of Fig. 5(b) ($E_{\min}/R = 0.253$, $q = 0.0359$ m^2/s), the deviation of results is small, but still appreciable. This computation sets the limit for application of the Saint-Venant theory at approximately $-h_c z_{bxx} = (2/3)(E/R) \approx 0.168$, or simply 0.15, in agreement with the results of Fig. 4. No explicit limit of application of the Saint-Venant theory for flow over variable topography appears to be previously available.

Water Wave Celerity, Minimum Specific Energy, and Flow Momentum in Unsteady Flow

The unsteady-flow motion corresponding to the steady water surface profiles of Fig. 3(a) is detailed in Fig. 6. Figs. 6(a, c, e, and g) show water and discharge profiles at computational times $t = 0.5$, 1.5, 2, and 3 s, respectively. The functions $E(x,t)$, $\mathsf{F}(x,t)$, and $S(x,t)$ are plotted for the same times in Figs. 6(b, d, f, and h). Note first that a shock is formed given the sudden rise in discharge [Fig. 6(a)], and a smooth unsteady flow without discontinuities follows at $t = 3$ s [Fig. 6(g)]. As observed, $E(x,t)$, $\mathsf{F}(x,t)$, and $S(x,t)$ are discontinuous as the shock propagates, with left-side variables affected by unsteady motion and right-side variables corresponding to the initial steady-state conditions. The values of $E(x,t)$, $\mathsf{F}(x,t)$, and $S(x,t)$ at crest vicinity are detailed in Fig. 7 for the previous simulation times. At time $t = 0.5$ s, the shock has not reached yet the crest [Fig. 6(a)] so $E(x,t)$, $\mathsf{F}(x,t)$, and $S(x,t)$ at the weir zone

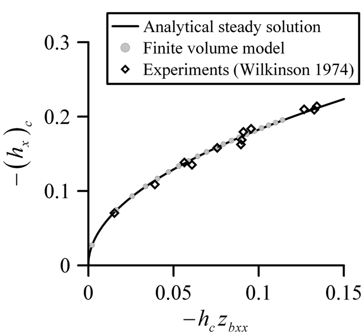

Fig. 4. Water surface slope at weir control section obtained from MUSCL-Hancock finite-volume model, analytical steady result [Eq. (4)], and experiments (data from Wilkinson 1974)

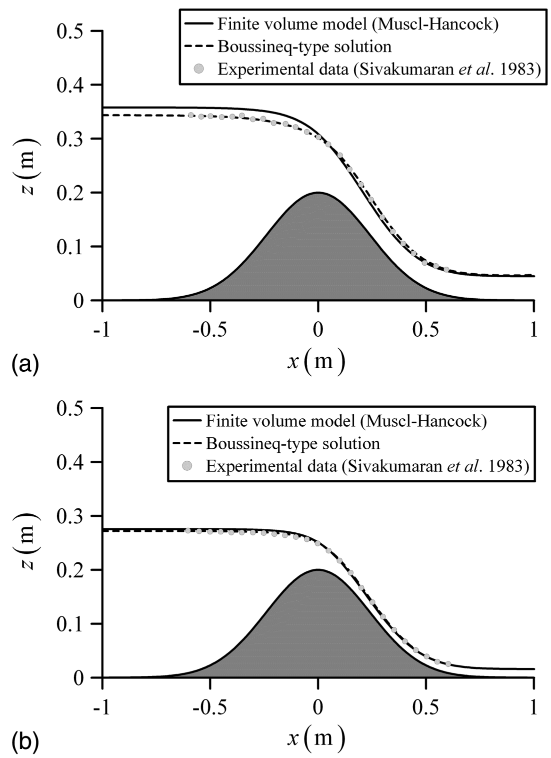

Fig. 5. Accuracy of shallow water, gradually varied flow theory over weir for (a) $E_{\min}/R = 0.516$; (b) $E_{\min}/R = 0.253$

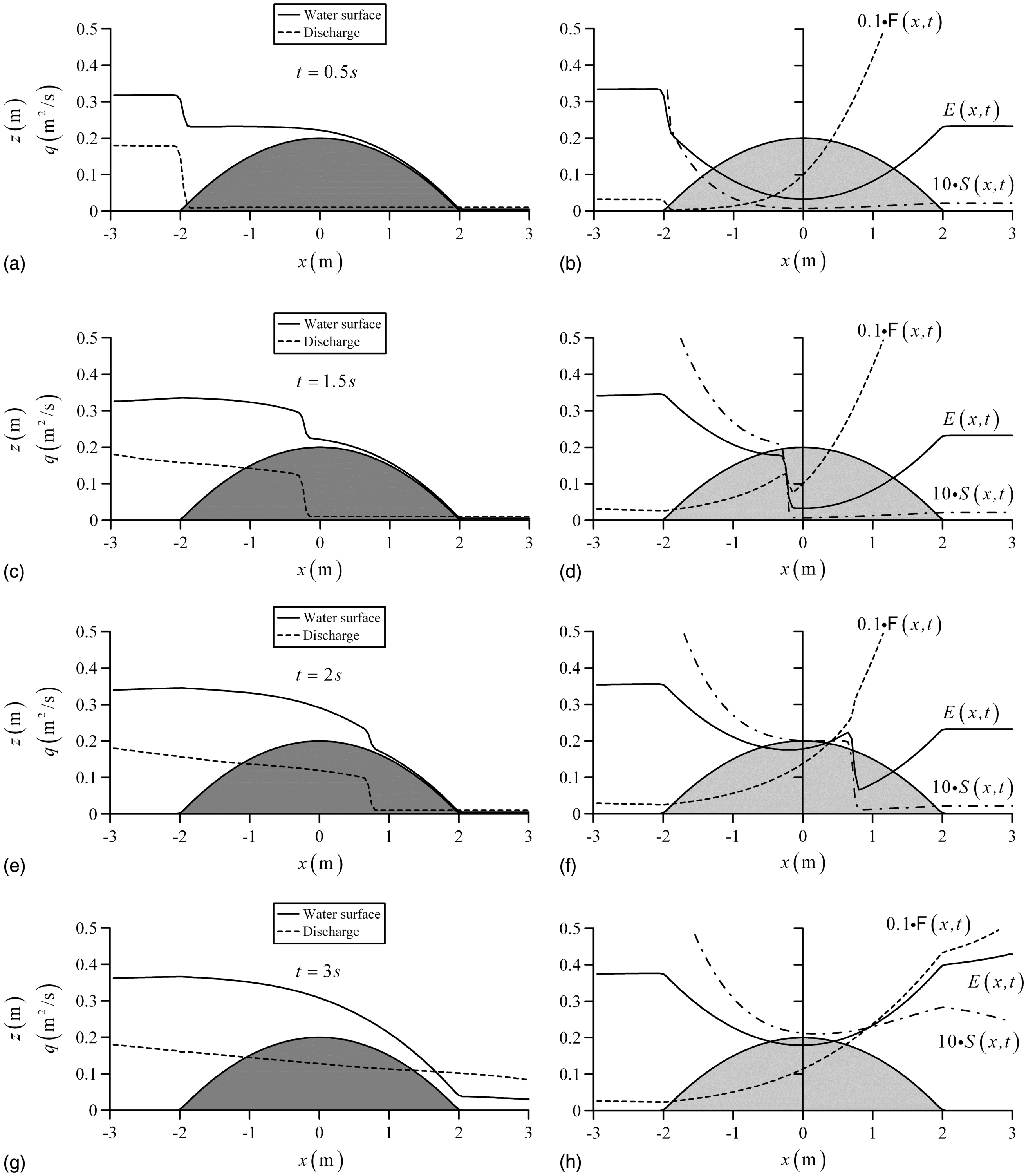

Fig. 6. Propagation of positive wave and temporal evolution of variables F, E, and S

are those of the initial steady flow [Fig. 7(a)]. At time $t = 1.5$ s, the discontinuity associated with the shock is near the crest [Fig. 7(b)], but the crest is not yet affected by the transient flow. At time $t = 2$ s, the shock front is at approximately $x = 0.9$ m, so the flow variables near the crest are effected by unsteadiness. The section of $E_{\min}$ is clearly not at the crest, and further different from the section where $\mathsf{F} = 1$. There is not a minimum in the S function at this instant of time. Computations at $t = 3$ s indicate that the entire computational domain is free from discontinuities in the solution [Fig. 6(g)], so all sections are affected by unsteadiness. The results of Fig. 7(d) are most revealing. The specific energy $E = E_{\min}$ occurs at the crest section ($x = 0$), but the condition $\mathsf{F} = 1$ is reached at a section $x < 0$. There is a minimum of specific momentum $S = S_{\min}$, but it is at a section $x > 0$. These results clearly reveal that the effect of unsteadiness provokes nonuniqueness of the critical flow concept, i.e., each critical flow definition is related to a different depth located at a different channel section, so that the traditional results are of no use in this paper. At $t = 50$ s the flow

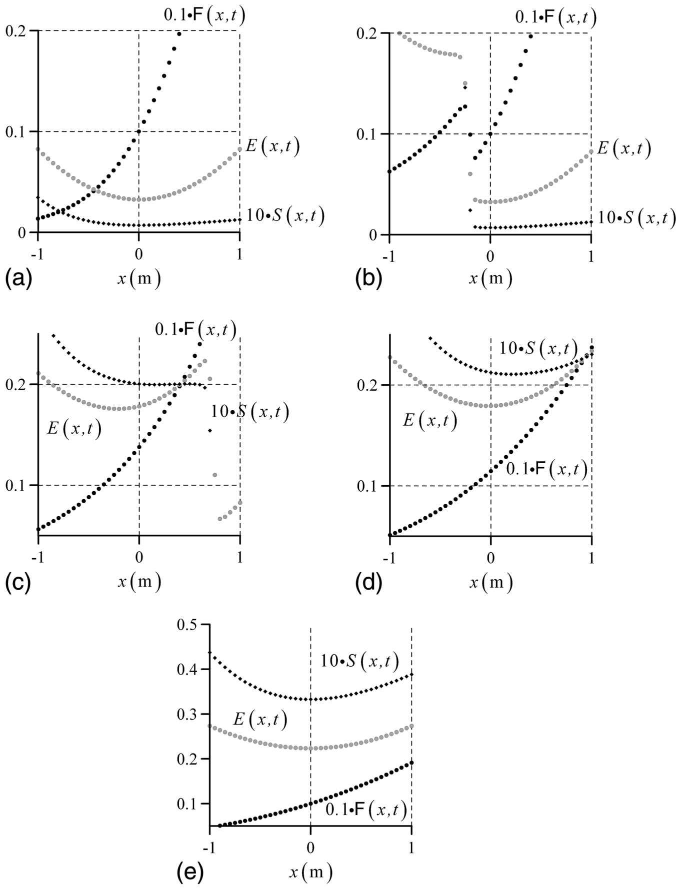

Fig. 7. Variables F, E, and S at crest zone during transient flow

is steady, and all definitions of critical flow converge with a single control section at the weir crest [Fig. 7(e)].

Unstable Transcritical Flow Profiles

In the singular point theory, Eq. (4) gives two roots (positive/negative), each associated with a different transcritical flow profile (Chow 1959; Montes 1998). The negative sign corresponds to the transition from subcritical to supercritical flow, already used in this paper in the former computations. It remains to investigate whether the inverse transition from supercritical to subcritical flow is likely to be of practical significance. Kabiri-Samani et al. (2014) demonstrated experimentally that the transition from supercritical to subcritical flow without a hydraulic jump is possible. Both experiments and steady-state singular point theory, therefore, support this transitional flow profile as a valid solution. The purpose of this section is to investigate whether this transition profile is robust and stable relative to unsteady-flow perturbations (as is the transition from subcritical to supercritical flow). The steady-state computations for this kind of transitional flow proceed with no problem just taking the positive root in Eq. (4). This was done for the weir test presented at Fig. 3. The water surface profiles for the initial discharge, and the target discharge of 0.18 $\mathrm{m^2/s}$ are plotted in Fig. 8(a). The question is whether the unsteady-flow computations produce the target steady profile of this transitional flow type, starting from another transition profile corresponding to the initial steady flow. For this test case, because the inlet flow is supercritical, two boundary conditions, depth and discharge, must be prescribed. These are supplied from the target steady-flow profile. At the outlet subcritical section, only the depth is specified; whereas the discharge is computed using ghost cells. The evolution of the unsteady-flow motion is depicted in Fig. 8, in which two shocks are formed [Figs. 8(b and c)] until they intersect at $t = 1.5$ s [Fig. 8(d)], thereby leading to a single shock propagating toward the inlet section [Figs. 8(e and f)]. If the boundary conditions at the inlet section are changed to permit the flow passage, a whole subcritical flow profile is finally formed over the weir once steady state is reached. The same behavior was obtained using small variations of the target steady state over the initial steady-flow profile. It was impossible to obtain the transcritical flow profile from $\mathsf{F} > 1$ to $\mathsf{F} < 1$ as the result of asymptotic unsteady-flow computations. In contrast, the reverse-transitional flow (i.e., Fig. 3) was always stable and convergent in unsteady-flow computations.

Rating Curve in Unsteady Flow

In steady flows, critical flow defined as the maximum discharge for a given E yields the rating curve (Montes 1998; Chanson 2004)

$$q_c = \left(\frac{2}{3}\right)^{3/2} (gE_c^3)^{1/2} \tag{24}$$

For weir flow E_c and q_c are specific energy and discharge at the crest section, respectively. This is a basic steady-state rating curve, assumed to apply for water discharge measurement purposes (Bos 1976) or to characterize outflow structures of dams (Montes 1998) (with correction coefficients as for nonhydrostatic pressure if the flow curvature is high). To test its accuracy during unsteady flows, the values of $E_c(t)$ and $q_c(t)$ for the weir flow problem shown in Fig. 3 were computed. Eq. (24) and the unsteady-flow results are shown in Fig. 9. The first unsteady point corresponding to the initial steady flow ($q = 0.01\ \mathrm{m^2/s}$) lies on Eq. (24). As soon as the shock waves pass the crest section, and the flow there becomes unsteady, the unsteady crest rating curve deviates from Eq. (24), physically implying that the value of q_c is not a maximum for E_c. As the unsteady flow tends to the new steady state corresponding to $q = 0.18\ \mathrm{m^2/s}$, the unsteady data point tends to lie on Eq. (24). The zone of $\pm 5\%$ of deviation in q relative to Eq. (24) is plotted in Fig. 9. A significant part of the unsteady rating curve is outside this domain, rendering Eq. (24) inaccurate for water discharge measurements purposes during the entire unsteady-flow motion. Unsteady-flow data of Chanson and Wang (2013) yielded a rating curve for a V-notch weir close to steady flow, despite the highly rapid flow motion in their experiments. However, the problem investigated in this paper is different, involving a shock wave propagating over the weir crest [Figs. 6(c and e)]. The flow just behind the shock induced a strong unsteadiness effect on the weir crest conditions [i.e., Fig. 6(e) for $t = 2$ s]. Thus, the flow profile over the weir crest is continuous ($\partial h/\partial x$ is finite) with a strong effect of unsteadiness on both q_c and E_c induced by the shock wave propagating in the tailwater weir face. At time $t = 3$ s [Fig. 6(g)], there are no shocks in the computational domain and the unsteady rating curve is within $\pm 5\%$ of deviation for the steady rating curve (Fig. 9).

Discussion

Saint-Venant equations produce realistic free-surface profile solutions across the critical depth using shock-capturing numerical methods. The computation of a steady-flow profile using an unsteady-flow computation produces a solution that automatically crosses the critical depth. This unsteady-flow computation is performed without any further special treatment at the critical point, because the unsteady computation does not suffer from

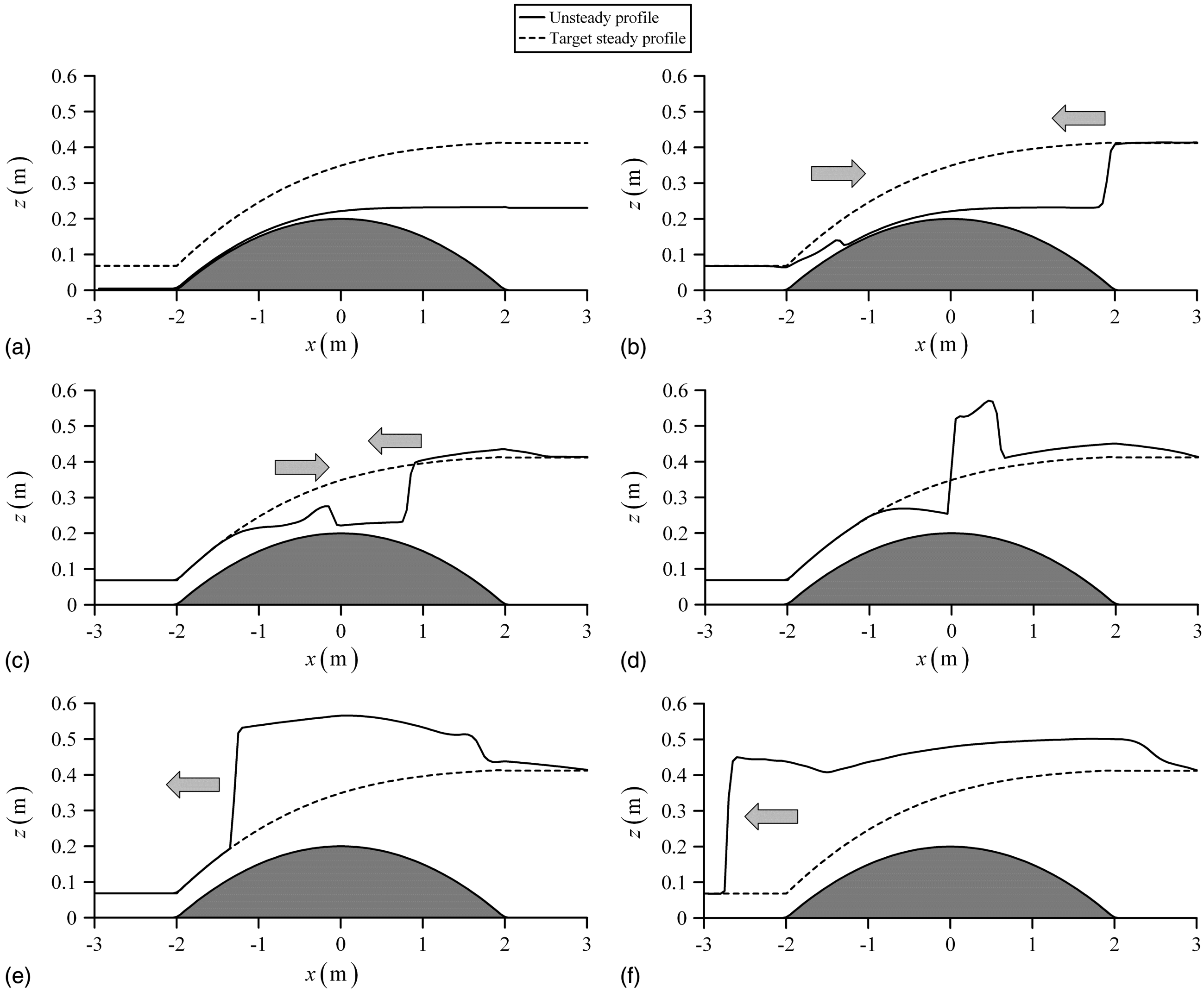

Fig. 8. Unstable transcritical flow profile from supercritical to subcritical flow during unsteady flow

any mathematical indetermination. However, the steady backwater equation has an indetermination at critical-flow conditions that must be resolved using L'Hopital's rule. The unsteady computation produces such singular point asymptotically as the steady state is approached.

The steady free-surface slope for the transition from subcritical to supercritical flow, computed from the unsteady-flow model, perfectly matches the analytical solution for steady flow obtained using L'Hospital's rule. It indicates the unsteady-flow model produces automatically such a critical point gradient in the computational domain to pass across the critical depth. The Saint-Venant equations are mathematically valid at the critical depth over variable topography. However, this model is physically inaccurate if the flow curvature is high, with the threshold value of $-h_c z_{bxx} = 0.15$.

During a transient flow, the positions of the points corresponding to $E = E_{\min}$, $S = S_{\min}$, and $\mathsf{F} = 1$ are different, and none is located at the weir crest. Once a steady flow is reached, all definitions of critical flow converge with a unique control section at the weir crest. Thus, the time variable produces nonuniqueness of the critical-depth concept with three different critical points in the computational domain, each consistent with a definition of critical flow. The relevant definition for unsteady flow is $U = (gh)^{1/2}$ (for a rectangular channel), which is coherent with momentum conservation and the singularity of the equations of motion, as suggested by Liggett (1993) without proof. It indicates that the minimum specific energy is a steady-state concept, a point so far not revealed in the literature, to the authors' knowledge. The notion of critical flow, as defined from the specific energy minimum, has little use in unsteady flow but is a fundamental tool for steady flows. In addition to the numerical results presented in this paper, a mathematical

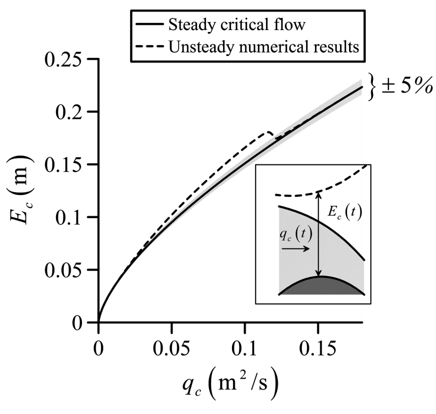

Fig. 9. Comparison of steady rating curve with results of unsteady flow computation

proof of divergence between the conditions $U = (gh)^{1/2}$ and $E = E_{\min}$ is provided (Appendix).

Starting unsteady-flow computations, with a transitional profile from $\mathsf{F} < 1$ to $\mathsf{F} > 1$, results in a new stable transcritical flow profile after applying a perturbation at the inlet section in the form of a discharge pulse. The same type of computation was conducted for the inverse transcritical flow profile from $\mathsf{F} > 1$ to $\mathsf{F} < 1$, which is also theoretically possible within the singular point theory. However starting with this kind of steady transcritical flow profile, and inducing perturbations compatible with a new transitional profile from $\mathsf{F} > 1$ to $\mathsf{F} < 1$ (corresponding to a different steady discharge), provokes unsteady-flow profiles that do not result in a new transcritical flow profile (from $\mathsf{F} > 1$ to $\mathsf{F} < 1$) as the steady-flow condition is reached. Hence, the transition from supercritical to subcritical flow over variable topography (without a hydraulic jump) is an unstable steady-flow profile relative to small unsteady-flow perturbations. Possibly, this flow profile is generated using very delicate adjustments of boundary conditions, but the present results indicate that this is not likely to be a natural profile in real-life conditions.

A weir crest is a discharge meter in steady flow, where the rating curve is given by the maximum discharge principle. During unsteady flow, the relationship between E and q at the weir crest does not follow the steady rating curve, thereby indicating that it is not a control section. Physically, it indicates that if a discharge equation is defined on the basis of the crest section, then the discharge coefficient and the ratio of crest depth to specific energy depend on time and not constant values as obtained in the classical steady-state analysis. From a practical standpoint, this may have severe implications because deviations of the real unsteady rating curve from the steady rating curve may not be acceptable for water discharge measurement purposes. Thus, the major finding is that Eq. (24) is never verified exactly in unsteady flow over a weir. As long as there are shocks in any point of the computational domain downstream from the weir crest, the unsteadiness effect is strong and deviations of the unsteady rating curve from Eq. (24) are unacceptable. However, if the instantaneous water surface profile is free from shocks, deviations of the unsteady rating curve from the critical depth rating curve are acceptable.

Conclusions

Unsteady computations of transcritical flow over variable bed topography were conducted using weir flow as a representative case. Comparison of asymptotic unsteady-flow profiles with steady flow backwater computations indicates that the Saint-Venant equations produce a singular point during the transient flow to cross critical points. This states that the singular point method is a steady technique to mathematically resolve the existence of these indeterminations, which, in turn, are automatically computed with unsteady-flow models. This demonstrates the general validity of the singular point method and that the steady backwater equation is mathematically valid at a critical point. However, although mathematically valid, the outcome of the gradually varied flow model is accurate only if the flow curvature in the vicinity of the critical depth is small.

Unsteady numerical flow computations reveal that the section isolated from water waves $[U = (gh)^{1/2}]$ is generally different from the sections where the specific energy and the specific momentum reach minimum values. An analytical proof of the divergence of results is also given. This leads to the conclusion that the only relevant definition of critical flow for both unsteady and steady flow is $\mathsf{F} = U(x,t)/[gh(x,t)]^{1/2} = 1$, which exhibits singularities in the equations of motion. Consequently, the minimum specific energy and force are steady-flow concepts of little use in unsteady flow, although they are important tools for steady-flow computations.

Computation of the relationship between the discharge and specific energy at the weir crest during unsteady flow revealed that the maximum discharge principle is not verified. Therefore, use of crest sections as discharge meters during unsteady flows needs to be done with caution because the effect of unsteadiness may induce appreciable errors that are, however, acceptable if the flow is free from shocks.

This paper was designed as an educational piece of work from which is concluded that the general definition of critical flow implies a section where the flow is isolated from water waves (valid for both unsteady and steady flows), as stated by Liggett (1993). The specific energy is a powerful steady-state concept, with a minimum value coincident with the definition of critical flow originating from the equations of motion, if these are detailed to steady flow. Thus, minimum specific energy and momentum should, henceforth, not be used to define critical flow but rather quoted as particular cases in which the simplification of critical flow to steady state regain an additional physical meaning.

Appendix. Minimum Specific Energy and Water Wave Celerity in Unsteady Flow

The specific energy is a function $E = E(h,q)$, where both h and q are functions of (x,t). The total variation of E is generally given by

$$dE = \frac{\partial E}{\partial h}dh + \frac{\partial E}{\partial q}dq \tag{25}$$

Further, the partial differentials of E are with Eq. (2)

$$\frac{\partial E}{\partial h} = 1 - \frac{q^2}{gh^3}, \qquad \frac{\partial E}{\partial q} = \frac{q}{gh^2} \tag{26}$$

Now, q and h vary in the (x,t) plane according to

$$dq = \frac{\partial q}{\partial x}dx + \frac{\partial q}{\partial t}dt, \qquad dh = \frac{\partial h}{\partial x}dx + \frac{\partial h}{\partial t}dt \tag{27}$$

Combining Eqs. (25)–(27) results in

$$dE = \left(1 - \frac{q^2}{gh^3}\right)\left(\frac{\partial h}{\partial x}dx + \frac{\partial h}{\partial t}dt\right) + \frac{q}{gh^2}\left(\frac{\partial q}{\partial x}dx + \frac{\partial q}{\partial t}dt\right) \tag{28}$$

The derivative dE/dh is thus given by the general equation

$$\frac{dE}{dh} = \left(1 - \frac{U^2}{gh}\right)\frac{dt}{dh}\left(\frac{\partial h}{\partial x}\frac{dx}{dt} + \frac{\partial h}{\partial t}\right) + \frac{U}{gh}\frac{dt}{dh}\left(\frac{\partial q}{\partial x}\frac{dx}{dt} + \frac{\partial q}{\partial t}\right) \tag{29}$$

Based on Eq. (29), it is demonstrated that if $dx/dt = 0$, that further implies $\mathsf{F} = U/(gh)^{1/2} = 1$, it does not result in an extreme of the specific energy $dE/dh = 0$ in unsteady flow because the term $\partial q/\partial t \neq 0$.

Acknowledgments

The authors are very much indebted to Dr. Sergio Montes, University of Hobart, Tasmania, for his advice on this research. The first author is further grateful to Dr. L. Mateos, IAS-CSIC, for his comments at several stages of this research work. This paper was supported by the Spanish project CTM2013-45666-R, Ministerio de Economía y Competitividad and by the Australian Research Council (Grant DP120100481).

Notation

The following symbols are used in this paper:

A = area of finite volume (m^2);
a = shallow-water wave celerity = $(gh)^{1/2}$ (m/s);
CFL = Courant-Friedrichs-Lewy number (-);
E = specific energy head (m);
$\mathbf{F}$ = vector of fluxes (m^2/s, m^3/s^2);
F = Froude number (-);
g = gravity acceleration (m/s^2);
H = total energy head (m);
h = flow depth measured vertically (m);
h_c = critical depth for parallel-streamlined flow $(m) = (q^2/g)^{1/3}$;
h^* = intermediate flow depth in Riemann problem (m);
i = cell index in x-axis (-);
k = index (-);
n = node index in t-axis (-);
$\mathbf{Q}$ = alternative vector of conserved variables (m, m^2/s);
q = unit discharge (m^2/s);
q_L, q_R = auxiliary variables (-);
R = crest radius of curvature (m);
$\mathbf{S}$ = vector of source terms (m/s, m^2/s^2);
S = specific force (or momentum) (m^2);
S_f = friction slope (-);
S_L, S_R = slope of characteristics lines (negative and positive) in Riemann problem (-);
S_o = channel bottom slope (-);
t = time (s);
$\mathbf{U}$ = vector of conserved variables (m, m^2/s);
U = mean flow velocity $(m/s) = q/h$;
x = horizontal distance (m);
z_b = channel bottom elevation (m);
z_s = free surface elevation (m);
Φ^+, Φ^- = limiter matrices (-); and
Ω = control volume (m^3).

Subscripts

c = crest section;
L = left state in Riemann problem;
min = minimum value; and
R = right state in Riemann problem.

References

Apelt, C. J. (1983). “Hydraulics of minimum energy culverts and bridge waterways.” *Aust. Civ. Eng. Trans., I.E. Aust.*, CE25(2), 89–95.

Aureli, F., Maranzoni, A., Mignosa, P., and Ziveri, C. (2008). “A weighted surface-depth gradient method for the numerical integration of the 2D shallow water equations with topography.” *Adv. Water Resour.*, 31(7), 962–974.

Bakhmeteff, B. A. (1912). “O neravnomernom wwijenii jidkosti v otkrytom rusle [Varied flow in open channels].” St Petersburg, Russia (in Russian).

Bakhmeteff, B. A. (1932). *Hydraulics of open channels*, McGraw-Hill, New York.

Bélanger, J. B. (1828). *Essai sur la solution numérique de quelques problèmes relatifs au mouvement permanent des eaux courantes [On the numerical solution of some steady water flow problems]*, Carilian-Goeury, Paris (in French).

Blau, E. (1963). *Der Abfluss und die hydraulische Energieverteilung über einer parabelförmigen Wehrschwelle [Distributions of discharge and energy over a parabolic-shaped weir]*, Mitteilungen der Forschungsanstalt für Schiffahrt, Wasser- und Grundbau, Berlin, Heft 7, 5–72 (in German).

Bos, M. G. (1976). *Discharge measurement structures*, International Institute for Land Reclamation (ILRI), Wageningen, Netherlands.

Castro-Orgaz, O. (2013). “Potential flow solution for open channel flows and weir crest overflows.” *J. Irrig. Drain. Eng.*, 10.1061/(ASCE)IR.1943-4774.0000580, 551–559.

Chanson, H. (2004). *The hydraulics of open channel flows: An introduction*, Butterworth-Heinemann, Oxford, U.K.

Chanson, H. (2006). “Minimum specific energy and critical flow conditions in open channels.” *J. Irrig. Drain. Eng.*, 10.1061/(ASCE)0733-9437(2006)132:5(498), 498–502.

Chanson, H., and Montes, J. S. (1998). “Overflow characteristics of circular weirs: Effects of inflow conditions.” *J. Irrig. Drain. Eng.*, 10.1061/(ASCE)0733-9437(1998)124:3(152), 152–162.

Chanson, H., and Wang, H. (2013). “Unsteady discharge calibration of a large V-notch weir.” *Flow Meas. Instrum.*, 29, 19–24.

Chaudhry, M. H. (2008). *Open-channel flow*, 2nd Ed., Springer, New York.

Chen, J., and Dracos, T. (1996). “Water surface slope at critical controls in open channel flow.” *J. Hydraul. Res.*, 34(4), 517–536.

Chow, V. T. (1959). *Open channel hydraulics*, McGraw-Hill, New York.

Escoffier, F. F. (1958). “Transition profiles in nonuniform channels.” *Trans. ASCE*, 123, 43–56.

Hager, W. H. (1985). “Critical flow condition in open channel hydraulics.” *Acta Mechanica*, 54(3–4), 157–179.

Hager, W. H. (1999). *Wastewater hydraulics: Theory and practice*, Springer, Berlin.

Henderson, F. M. (1966). *Open channel flow*, MacMillan, New York.

Iwasa, Y. (1958). “Hydraulic significance of transitional behaviours of flows in channel transitions and controls.” *Memoires of the faculty of engineering*, Kyoto Univ., Kyoto, Japan, 237–276.

Jaeger, C. (1949). *Technische hydraulik [Technical hydraulics]*, Birkhäuser, Basel, Switzerland (in German).

Jain, S. C. (2001). *Open channel flow*, Wiley, New York.

Kabiri-Samani, A., Hossein Rabiei, M., Safavi, H., and Borghei, S. M. (2014). “Experimental-analytical investigation of super- to subcritical flow transition without a hydraulic jump.” *J. Hydraul. Res.*, 52(1), 129–136.

LeVeque, R. J. (2002). *Finite volume methods for hyperbolic problems*, Cambridge University Press, New York.

Liggett, J. A. (1993). “Critical depth, velocity profile and averaging.” *J. Irrig. Drain. Eng.*, 10.1061/(ASCE)0733-9437(1993)119:2(416), 416–422.

Liggett, J. A. (1994). *Fluid mechanics*, McGraw-Hill, New York.

Massé, P. (1938). “Ressaut et ligne d´eau dans les cours à pente variable [Hydraulic jump and free surface profile in channels of variable slope].” *Rev. Gén. Hydr.*, 4(19), 7–11; 4(20), 61–64 (in French).

Matthew, G. D. (1991). “Higher order one-dimensional equations of potential flow in open channels.” *Proc. ICE*, 91(2), 187–201.

Montes, J. S. (1994). “Potential flow solution to the 2D transition from mild to steep slope.” *J. Hydraul. Eng.*, 10.1061/(ASCE)0733-9429(1994)120:5(601), 601–621.

Montes, J. S. (1998). *Hydraulics of open channel flow*, ASCE, Reston, VA.

Poincaré, H. (1881). “Mémoire sur les courbes définies par une équation différentielle [Memoir on the defined curves of a partial differential equation].” *J. Math. Pures Appl.*, 7, 375–422 (in French).

Sivakumaran, N. S., Tingsanchali, T., and Hosking, R. J. (1983). “Steady shallow flow over curved beds.” *J. Fluid Mech.*, 128(1), 469–487.

Stoker, J. J. (1957). *Water waves: The mathematical theory with applications*, Interscience, New York.

Sturm, T. W. (2001). *Open channel hydraulics*, McGraw-Hill, New York.
Toro, E. F. (1997). *Riemann solvers and numerical methods for fluid dynamics*, Springer, London.
Toro, E. F. (2002). *Shock-capturing methods for free-surface shallow flows*, Wiley, Singapore.
von Kármán, T., and Biot, M. A. (1940). *Mathematical methods in engineering: An introduction to mathematical treatment of engineering problems*, McGraw-Hill, New York.
Vreugdenhil, C. B. (1994). *Numerical methods for shallow water flow*, Kluwer, Norwell, MA.
Wilkinson, D. L. (1974). "Free surface slopes at controls in channel flow." *J. Hydraul. Div.*, 100(8), 1107–1117.
Wilson, E. H. (1969). "Surface profiles in non-prismatic rectangular channels." *Water Power*, 21(11), 438–443.
Yen, B. C. (1973). "Open-channel flow equations revisited." *J. Eng. Mech. Div.*, 99(5), 979–1009.
Yen, B. C. (1975). "Further study on open-channel flow equations." *SFB 80/T/49*, Universität Karlsruhe, Karlsruhe, Germany.
Ying, X., Khan, A., and Wang, S. (2004). "Upwind conservative scheme for the Saint Venant equations." *J. Hydraul. Eng.*10.1061/(ASCE)0733-9429(2004)130:10(977), 977–987.
Zhou, J. G., Causon, D. M., Mingham, C. G., and Ingram, D. M. (2001). "The surface gradient method for the treatment of source terms in the shallow water equations." *J. Comput. Phys.*, 168(1), 1–25.